MODELLING CANDU FUEL ELEMENT AND BUNDLE BEHAVIOUR FOR PERFORMANCE OF INTACT AND DEFECTIVE FUEL

K. Shaheen*, J.S. Bell, A. Prudil, and B.J. Lewis
Department of Chemistry and Chemical Engineering
Royal Military College of Canada
17000 Station Forces, Kingston, Ontario, Canada K7K 7B4
*Corresponding Author: E-mail – Khaled.Shaheen@gmail.com

Abstract

The FORCE code simulates fuel element performance. Temperature, gas pressure, and sheath strain predictions in an intact element are consistent with the ELESTRES and ELESIM codes. Defective fuel performance predictions show reasonable agreement with coulometric titration fuel stoichiometry data and coolant activity concentration measurements from CRL experiments. A bundle deformation model, assuming a beam element, accurately reproduces verification cases which characterize the BOW code. The addition of endplate interaction is used to simulate an out-reactor deformation experiment conducted by AECL with reasonable agreement. A pellet deformation model demonstrates a capability to analyze pellet-to-pellet and pellet-sheath interaction within an intact element.

1. Introduction

Industry codes such as ELESTRES [1], ELOCA [2], and BOW [3] are used to simulate fuel behaviour. The goal of the current work is to test the ability of platform-based models as tools to predict fuel performance.

Nuclear fuel performance in an individual element is dependent on a number of inter-related phenomena, including fission heating and heat transport, fission gas release from the evolving uranium dioxide fuel grains and diffusion to the fuel-to-sheath gap, and material deformation of both the fuel and the Zircaloy sheath. Bundle behavior involves bowing of individual elements, which is primarily thermally induced [4,5], as well as the effects of contact between different elements and the bundle endplates. With the rare incidence of a sheath defect, coolant flow into the fuel element results in fuel oxidation, which in turn affects the fission gas release from the fuel element [6] and the fuel thermal performance [7].

2. Model Development

Three models are described in this work: (i) the FORCE (Fuel Operational peRformance Computations in an Element) code for intact and defective fuel element performance (Section 2.1); (ii) a bowing model, based on a beam approximation, to predict the overall deflection of an element due to an external load (Section 2.2); and (iii) a more detailed pellet and sheath deformation model (Section 2.3). The overall objective of the current work is to develop these models on a commercial numerical platform, COMSOL Multiphysics [8] (henceforth 'Comsol'), so that the individual phenomena/codes describing fuel-element performance, fuel

element/bundle bowing, and pellet deformation can potentially be linked into a single multiphysics tool.

2.1 The FORCE code

2.1.1 Heat generation and transport

The heat conduction equation in the fuel element is given by [9, 10]:

$$\rho C_p \frac{\partial T}{\partial t} = \bar{\nabla} \cdot \left(k \bar{\nabla} T\right) + \frac{P_{lin}}{\pi a_p^2} \left(\frac{\kappa a_p \left(I_0(\kappa r) + \beta_{Pu} e^{\lambda_{Pu}(r - a_p)} \right)}{2\left(I_1(\kappa a_p) + \beta_{Pu} e^{-\lambda_{Pu} a_p} \frac{\kappa}{\lambda_{Pu}^2 a_p} + \beta_{Pu} \frac{\kappa}{\lambda_{Pu}} - \beta_{Pu} \frac{\kappa}{\lambda_{Pu}^2 a_p} \right)} \right) \quad (1)$$

where r is the radial coordinate, t is time, and T is temperature. The term P_{lin} is the element power rating, a_p is the pellet radius, κ is the inverse neutron diffusion length, the Bessel functions I_0 and I_1 account for neutron flux depression, and the terms β_{Pu} and λ_{Pu} account for the buildup of plutonium on the outer surface of the fuel. The heat generation term applies within the fuel pellet but not in the sheath. The terms ρ, C_p, and k represent density, heat capacity, and thermal conductivity, which vary between the fuel and sheath.

Over time, fuel expansion and sheath creepdown bring the fuel and sheath into contact. Due to surface roughness, heat transfer from the fuel pellet to the sheath occurs via both gas conduction and solid-to-solid conduction. In the FORCE code, these two modes of heat transfer are captured using an effective thermal conductivity given by:

$$k_{eff} = \frac{h_{solid} + h_{gas}}{h_{gas}} k_f \quad (2)$$

where the terms h_{solid} and h_{gas} represent the solid-to-solid and solid-to-gas contributions to the fuel-to-sheath transfer, respectively, and k_f is the thermal conductivity of the gas. The term h_{solid} takes effect only during fuel-to-sheath contact, assumed to occur when the gap thickness equals the root-mean-square surface roughness as defined above.

The temperature at the sheath outer surface is dependent on heat transfer from the coolant:

$$T_{so} = T_c + \frac{P_{lin}}{2\pi} \frac{1}{r_{so} h_{sc}} \quad (3)$$

Here T_c is the coolant temperature r_{so} is the sheath outer radius, and h_{sc} is the sheath-to-coolant heat transfer coefficient.

2.1.2 Fission Gas Diffusion and Grain Growth

The fractional release of stable fission gases to the fuel grain surface is predicted using the Booth diffusion equation, which approximates the grains as spheres, as solved analytically by Kidson [11]. For a single power cycle, the Kidson solution reduces to that of Beck [12]:

$$F(t) = 1 - \left(\frac{6}{\pi^2}\right)\sum_{n=1}^{\infty}\left(\frac{1}{n^2}\right)e^{\left(\frac{-n^2\pi^2 D\cdot t}{a^2}\right)} \tag{4}$$

where D_g is the gas diffusion coefficient in the uranium dioxide grain, and d_g is the grain diameter (in micrometres), given by Khoruzii et. al. [13] as:

$$\frac{dd_g}{dt} = k_g\left(\frac{1}{d_g} - \frac{1}{d_{g,\max}} - \frac{\dot{F}T}{6.71\times10^{24}\exp(-5620/T)}\right) \tag{5}$$

where k_g is the grain growth rate term, and $d_{g,max}$ is the limiting grain size. The last term, where $\dot{F}$ is the fission rate, accounts for the retarding effect of irradiation on grain growth. As fission gas atoms are released to the fuel grain surface, they form lenticular bubbles along the grain boundaries. Over time, these bubbles can percolate to form a diffusion path to the fuel surface. The pellet release is thus given by the volumetric integral of:

$$N_{conc} = \begin{cases} \left(\int_0^t F(t)Bdt - N_{sat}\frac{3}{a}\right), & \int_0^t F(t)Bdt \geq N_{sat}\frac{3}{a} \\ 0, & \int_0^t F(t)Bdt < N_{sat}\frac{3}{a} \end{cases}, \tag{6}$$

where B is the production rate of fission gas atoms, which is given as a function of the fission rate $\dot{F}$ to be $0.25\dot{F}$, the term N_{sat} accounts for fission gas saturation on the grain surface as determined by White et. al. [14], and a is the grain radius.

2.1.3 Fuel Pellet Deformation

The strain in the fuel is a sum of thermal expansion (ε_{th}) [15], densification (ε_{dens}) [16], fission gas swelling (ε_{FG}) [17], and fission solid swelling (ε_{FS}) [18]. These strains are given by:

$$\varepsilon_{UO_2} = \varepsilon_{th} + \varepsilon_{dens} + \varepsilon_{FG} + \varepsilon_{FS} \tag{7}$$

$$\varepsilon_{th} = \begin{cases} 0.99734 + 9.802\times10^{-5}T - 2.705\times10^{-10}T^2 + 4.391\times10^{-13}T^3, 273K \leq T < 923K \\ 0.99672 + 1.179\times10^{-5}T - 2.429\times10^{-9}T^2 + 1.219\times10^{-12}T^3, T \geq 923K \end{cases} \tag{8}$$

$$\varepsilon_{dens} = 0.6 - \exp\left(-0.506 - 8.67\times10^{-10}T^3\left(1 - \exp\left(-2.867\times10^{-2}Bu\right)\right)\right) \tag{9}$$

$$\dot{\varepsilon}_{FG} = 9.42\times10^{-36}(2800\text{-}T)^{11.73}e^{-.0162(2800\text{-}T)}e^{-8\times10^{-7}\rho_{UO_2}Bu}\rho_{UO_2}\frac{dBu}{dt} \tag{10}$$

$$\varepsilon_{FS} = \frac{1}{3}0.0032\frac{Bu}{225} \tag{11}$$

where Bu is the average fuel burnup, determined by:

$$\frac{dBu}{dt} = \frac{P_{lin}M_{UO2}}{\pi\cdot a_p^2\rho_0 M_U} \tag{12}$$

Here M_{UO2} and M_U are the atomic masses of uranium dioxide and uranium, respectively, and ρ_0 is the as-fabricated density of uranium. The above strains are entered into a structural mechanics application mode in Comsol in order to solve for the fuel deformation.

2.1.4 Sheath Deformation

The thin sheath (inner-radius-to-wall-thickness ratio greater than 10) experiences deformation due to external coolant pressure and internal fuel expansion. The sheath deformation is a function of the hoop strain ε_s^{θ} [19]:

$$r_{si} = r_{si,0} e^{\varepsilon_\theta} \tag{13}$$

The hoop strain is the sum of thermal ($\varepsilon_{th}^{\theta}$) [18], elastic ($\varepsilon_{el}^{\theta}$) [19], and creep strains ($\varepsilon_{cr}^{\theta}$) [20, 21]:

$$\varepsilon_s^{\theta} = \varepsilon_{th}^{\theta} + \varepsilon_{el}^{\theta} + \varepsilon_{cr}^{\theta} \tag{14}$$

$$\varepsilon_{th}^{\theta} = \begin{cases} -2.073\times10^{-3} + 6.721\times10^{-6} T, & T < 1050\,\mathrm{K} \\ 1.486\times10^{-2} - 9.398\times10^{-6} T, & 1050\,\mathrm{K} \le T < 1270\,\mathrm{K} \\ -9.450\times10^{-3} + 9.7\times10^{-6} T, & T \ge 1270\,\mathrm{K} \end{cases} \tag{15}$$

$$\varepsilon_{el}^{\theta} = \frac{1}{E_{Zr}} \frac{r_{si}}{t_s} \left(P_{in} - P_{ex}\right) \left(1 - \frac{\nu_{Zr}}{2}\right) \tag{16}$$

$$\varepsilon_{cr}^{\theta} = 1.88\times10^{-2} \exp\left(-\frac{34726}{T}\right) \left(\frac{r_{si}}{t_s}\left(P_{in} - P_{ex}\right)\right)^{5.3} \frac{F - \frac{G}{2}}{\sqrt{\frac{F+G}{4} + H}} \tag{17}$$

where E_{Zr}, ν_{Zr}, F, G, and H represent the Young's modulus, Poisson's ratio, and Hill anisotropy parameters for the sheath, respectively. The difference between the internal and external pressures acting on the sheath is given by ($P_{in} - P_{ex}$).

2.1.5 Defective fuel oxidation and oxygen transport

The oxygen transport equation of the conceptual Higgs oxidation model [22] is implemented:

$$c_u \frac{\partial x}{\partial t} = c_u \vec{\nabla} \cdot \left(D_{ox} \left(\vec{\nabla} x + \frac{Q^*}{RT^2} \vec{\nabla} T \right) \right) + \sigma_{fuel} R_{reaction} \tag{18}$$

where x is the deviation from stoichiometry in $UO_{2\pm x}$, c_u is the molar density of the fuel, and D_{ox} is the diffusion coefficient for solid-state oxygen transport in the fuel. The flux term $\frac{Q^*}{RT^2}\nabla T$ accounts for diffusion of oxygen along a thermal gradient, i.e., the Soret effect. The term Q^* represents the heat of transport associated with this process. The term σ_{fuel} represents the surface-area-to-volume ratio of the fuel, and $R_{reaction}$ is the oxidation/reduction rate given by:

$$R_{reaction} = \begin{cases} R_{ox} = c_u \alpha_{ox} \sqrt{(1-q) p_t} \left(x_e - x\right), & x \le x_e \\ R_{red} = c_u \alpha_{ox} \sqrt{q p_t} \left(x - x_e\right), & x > x_e \end{cases} \tag{19}$$

The term c_u represents the molar density of uranium dioxide, α_{ox} represents the surface-exchange coefficient of oxygen between the fuel and the vapour, and p_t is the total gas pressure in the element (in atmospheres). The terms x_e and q represent the equilibrium stoichiometry deviation of the fuel and the hydrogen mole fraction of the vapour, respectively. These latter terms are fitted using empirical correlations given in references [22] and [23,24], respectively.

2.1.5 Fission gas release

The release of radioactive fission gases from the defective fuel element into the coolant, as predicted by the equations of the STAR (Steady-state and Transient Activity Release) code of El-Jaby et. al. [25], is integrated into the FORCE code. The intragranular diffusion of fission gases, including the effects of radioactive decay, is given in normalized coordinates ($\eta = r/a$):

$$\frac{\partial u(\eta,t)}{\partial t} = D' \frac{1}{\eta} \frac{\partial^2 (\eta u)}{\partial \eta^2} - \lambda u + y_c \dot{F} V_f \tag{20}$$

where u is given in number of atoms. $D' = \frac{D(x)}{a^2}$ is the dimensionless fission gas diffusion coefficient for hyperstoichiometric fuel, λ and y_c are the decay constant and cumulative yield of a given isotope, and V_f is the fuel volume. The release rate from the grain boundary is given by $R_{gr} = -3D' \left.\frac{\partial u}{\partial \eta}\right|_{\eta=1}$ and serves as the source term for the equation for fission gas inventory in the fuel-to-sheath gap:

$$\frac{dN_g}{dt} = R_{gr} - (\lambda + \nu) N_g \tag{21}$$

where ν is the escape rate coefficient of a given isotope from the gap to the coolant. The gap inventory in turn serves as the source term for the coolant inventory equation:

$$\frac{dN_c}{dt} = \nu N_g - (\lambda + \beta_p) N_c \tag{22}$$

where β_p is the purification rate coefficient for a given isotope in the primary coolant.

Given the constitutive equations outlined above with the associated thermophysical properties, fully detailed in references [24] and [26], the FORCE code can be solved for different operating scenarios.

2.2 Bundle deformation model development

Veeder and Schankula demonstrated that element deformation is predominately caused by temperature differences in the fuel pellet and sheath [27]. These temperature differences can lead to variations in the thermal expansion of the sheath and fuel materials, thereby producing thermal stress and strains. Temperature data from an intact fuel performance code can be used to determine these temperature differences and then be applied to solve for the deformation of a CANDU fuel element and fuel bundle. Similar work has been done by AECL in development of the BOW code [3]. Using the same basic assumptions as BOW the intent of this work is to implement a fuel element deformation model in hopes of using this as the basis for a fuel bundle deformation model using Comsol.

The geometry of a fuel element allows it to be treated mathematically like a beam. The premise behind a beam analysis is that because the length of the beam (in this case a fuel element) is roughly 50 times greater than its diameter (i.e., 50 cm in length compared to 1.31 cm in diameter), the deformation (and therefore the strain and stress) in the non-axial directions will be very small and can therefore be neglected (the cross section of the beam does not deform). This simplifies the analysis from examining stress in all three axes to only the stress and strain parallel to the length of the fuel element. In Comsol the deformation of a beam is solved by using an equilibrium condition called the virtual work principle. It is based on the assumption that the loads acting on a beam will do work in causing a displacement and that this energy is stored in the volume of the beam as stress. After applying the beam assumption to the virtual work principle can be expressed as [28]:

$$\delta W = \delta \int_L \left(M_y \frac{\partial \theta_y}{\partial s} + M_z \frac{\partial \theta_z}{\partial s} + M_x \frac{\partial \theta_x}{\partial s} + N \frac{\partial u_{axi}}{\partial s} \right) dx + \delta \int_V \mathbf{u}^T \mathbf{F} dV \tag{23}$$

Here M_y, M_z are the bending moments with units of Nm about y and z axis respectively, M_x is the torsional moment in Nm, θ is the angle to which the cross section has rotated to with respect to the x, y, and z axis in rad, N is the force acting perpendicular to the cross section in N, **u** is the displacement in m, u_{axi} is the displacement in direction perpendicular to the cross section and **F** is the external force loads in Nm^{-3}.

The interaction between fuel elements and endplates also needs to be accounted for. By assuming a small section of an endplate ring can be represented by a beam and that the endcap-to-endplate weld is "perfect", so that the elements and endplates act as if they are a continuous solid, the deformation of the endplates can therefore be used a boundary condition for the end(s) of the element as shown in Figure 1 below.

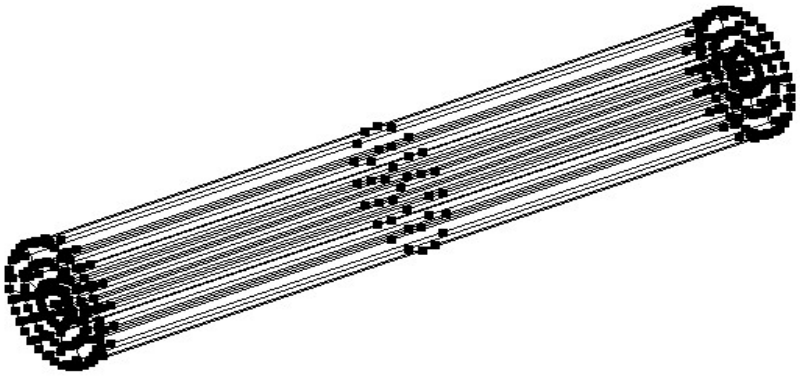

Figure 1 Endplate and sheath geometry of a 37 fuel element bundle approximated entirely by beams.

2.3 Pellet deformation model development

The FORCE code and the bundle deformation model treat the pellet stack as a uniform cylinder of UO_2 and do not explicitly account for the dishing and chamfering of the pellets on the solid-mechanics of the element. However, at the interface between pellets CANDU fuel sheaths are known to develop circumferential ridges due to the deformation of the pellet (i.e., pellet hour-glassing). The increased sheath strains which occur at these ridges are believed to be a contributing factor in fuel failures caused by Iodine-Stress-Corrosion Cracking (ISCC) [29]. A more detailed pellet model may therefore be useful in conjunction with other models by providing a method for predicting sheath strain at the pellet-to-pellet interface.

Increasing the complexity of the geometry necessitates increasing the density of mesh elements used in the finite element method to properly resolve the solutions. For this reason the pellet model includes a much smaller modeling volume than the FORCE code but with much greater mesh density. Symmetry of the fuel element was used to reduce the modeling volume to a single quarter-pellet modeled in the radial-axial plane (assuming azimuthal symmetry). This was accomplished using the symmetry planes shown in Figure 2(a) to obtain the model geometry shown in Figure 2(b). These symmetry planes were also used to establish the boundary conditions for three of the four edges of the model (with the boundary condition on the remaining edge, the sheath surface, being determined separately for each physics mode).

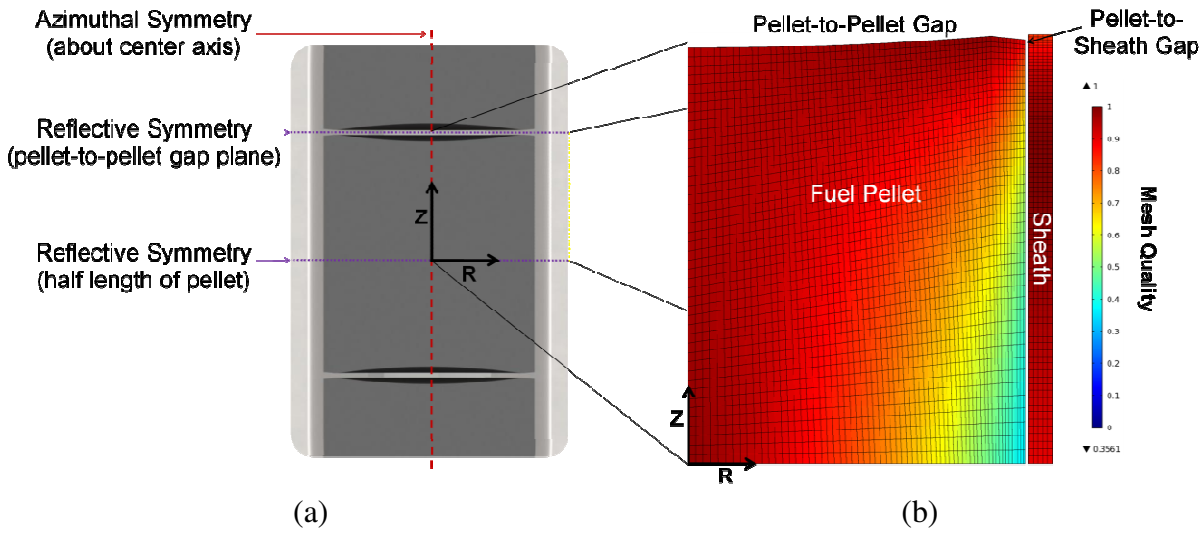

Figure 2: (a) Partial cross-section of a CANDU fuel element with overlay of assumed symmetry conditions and (b) surface plot of the model geometry and finite-element mesh quality (colour scale).

A number of improvements were made for the pellet deformation model, the largest of which is the localization of the pellet-to-sheath gap size and contact pressure. In the FORCE code the pellet and sheath are nearly uniform throughout the length of the element. This allows the FORCE code to use an element average pellet-to-sheath gap and contact pressure when calculating the heat-transfer coefficient. The pellet deformation model predicts variation of the gap size and contact pressure in the axial direction. Thus, the heat-transfer coefficient from the pellet to the sheath is calculated using the local values of the gap size and contact pressure.

In the pellet model contact between the pellet and the sheath is treated using a damped penalty method. The penalty method applies a force to each surface in the opposite direction as a function of the distance the boundaries have penetrated in to each other. The function is known as the penalty function. The larger the stiffness of the penalty function the greater the non-linearity of the model and the lower the penetration distance. A damping term may be added to improve convergence without changing the steady-state penetration distance. The damping term is a function of both the penetration distance and the time derivative of the penetration distance.

Since the contact pressure between the pellet and the sheath is expected to vary in the axial direction, a more robust treatment of the deformation of the sheath is needed. The semi-analytical treatment of the sheath solid-mechanics used in the FORCE code was replaced with a fully finite-element treatment. The FORCE code considers the sheath a thin-walled tube and the deformation is assumed to be uniform across the axial length of the element. Though the new treatment of the sheath is more computationally expensive it allows for a more detailed model where both the elastic and plastic sheath strains now vary with both radial and axial directions. This greater detail greatly improves the ability to model pellet-to-sheath interaction.

3. Results and Discussion

The results of the models for the FORCE code, fuel element bowing analysis and pellet deformation are described in the following sections.

3.1 FORCE code verification and validation

The results of the FORCE code for intact fuel performance are compared to those of the industry-standard toolset ELESTRES, as reported in reference [18], and the industry-produced code ELESIM, run for the same conditions. Predictions of temperature, gas pressure, and sheath hoop strain are compared. As seen in Figure 3, the FORCE code predictions show similar agreement with the ELESTRES and ELESIM codes at different linear power fuel ratings, and clearly lie between the predictions of the two codes for gas pressure at 55 kW m^{-1}.

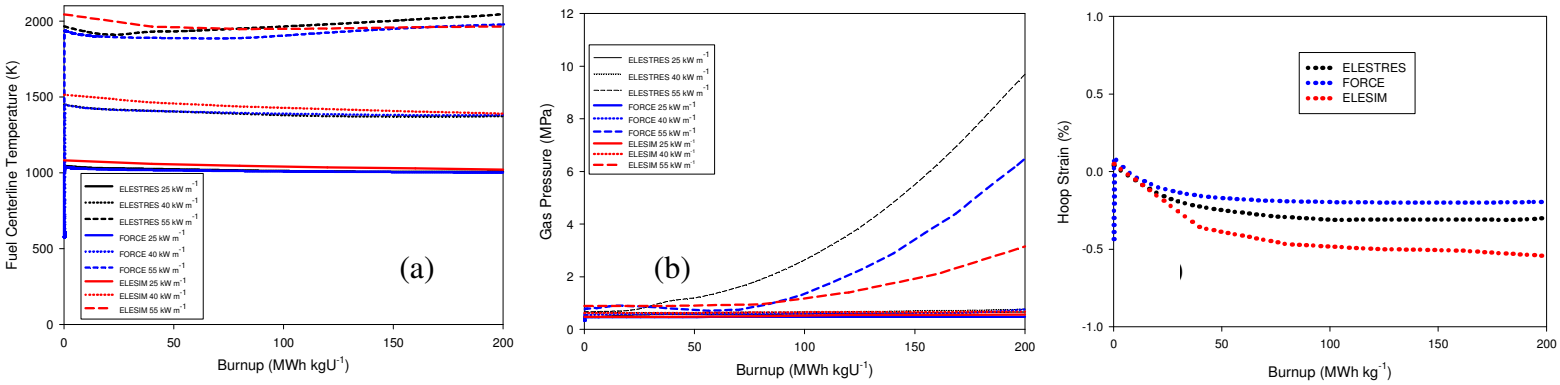

Figure 3 Comparison of (a) centerline temperature and (b) internal gas pressure and (c) sheath hoop strain predictions using the FORCE code and the ELESTRES and ELESIM codes.

The defective fuel oxidation model in the FORCE code is validated using coulometric titration data from Chalk River Laboratories for ten commercial defective elements [30]. One case is shown in Figure 4 below, demonstrating reasonable agreement between the FORCE code and both the experimental data and the conceptual model of Higgs et. al. [22], which is used to benchmark the correlations for hydrogen mole fraction [23, 24] used in the FORCE code:

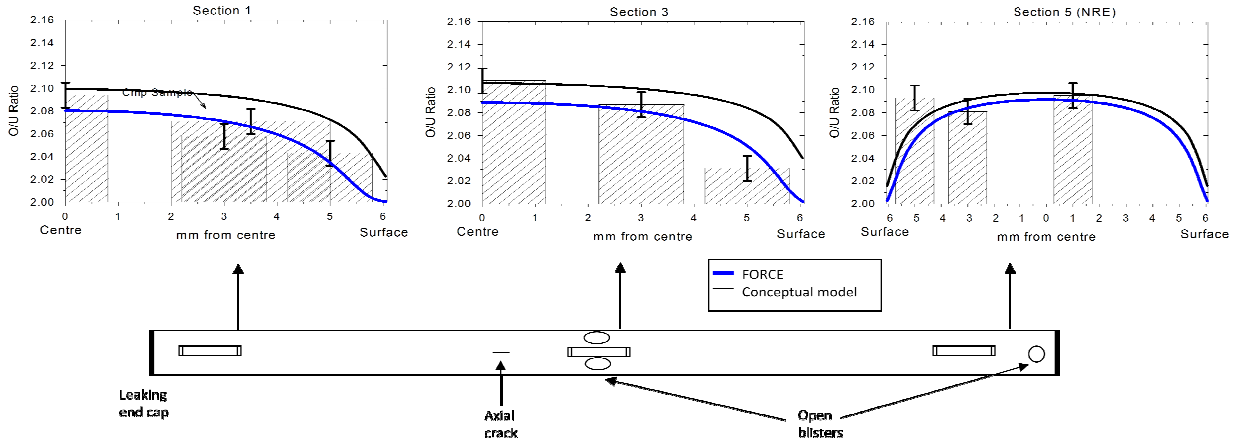

Figure 4 Comparison of radial profiles of oxygen-to-uranium ratio as given by the FORCE code, the conceptual Higgs fuel oxidation model, and the coulometric titration data of CRL for element X91.

The FORCE code is also used to predict the coolant activity concentration in power cycling experiments performed in the X-2 loop at the NRX reactor at Chalk River Laboatories [31] as

shown in Figure 5 below. The FORCE code shows reasonable agreement with both the STAR code [25] and the experimental data, while demonstrating some conservatism in the case of xenon-133.

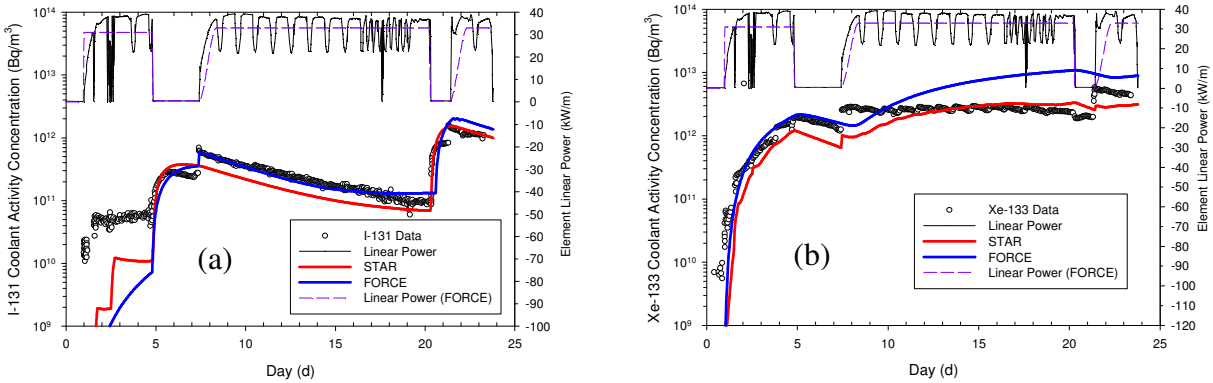

Figure 5 Comparison of coolant activity concentrations of (a) iodine-131, and (b) xenon-133 as given by the FORCE code, the STAR code of El-Jaby et. al., and the experimental measurements of CRL for experiment FFO-109-2.

The FORCE code is therefore shown to be in reasonable agreement with other codes and experimental data for both intact and defective nuclear fuel performance.

3.2 Bundle deformation verification and validation

In order to determine that the fuel element deformation model in COMSOL is capable of producing reasonable results, it was used to simulate verification cases used to characterize BOW. The results of two simulation cases are presented in Table 1. The results from the model implemented with Comsol are within 2% from the theoretical calculations.

Table 1 Two verification cases performed in the analysis of the BOW code taken from [3] compared to results from Comsol model.

Case Number	Case Description	Maximum Horizontal Deflection (mm)			Maximum Vertical Deflection (mm)		
		Theory	BOW	Comsol	Theory	BOW	Comsol
1	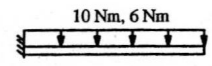	3.367	3.369	3.368	2.020	2.021	2.021
2	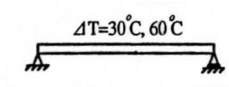	0.328	0.329	0.335	0.656	0.658	0.669
Case 1: The fuel element geometry has one end fixed while a 10 Nm moment is applied horizontally and a 6 Nm moment is applied vertically.							
Case 2: The fuel element geometry is simply supported at both ends and a temperature gradient of 30 K is applied horizontally and a 60 K applied vertically.							

This model was used to simulate an out-of-reactor bundle deformation experiment conducted by AECL Sheridan Park [3]. The experiment consisted of taking an unirradiated CANDU 6 fuel bundle at room temperature, and displacing an outer ring fuel element away from the fuel bundle at the mid-plane of the fuel element, where the applied force was varied up to about 45 N. Figure 6 compares the results of the simulation for the displacement at the mid-plane of the loaded fuel element to the experimental results. The results of the simulation are within 20% difference from the experimental results.

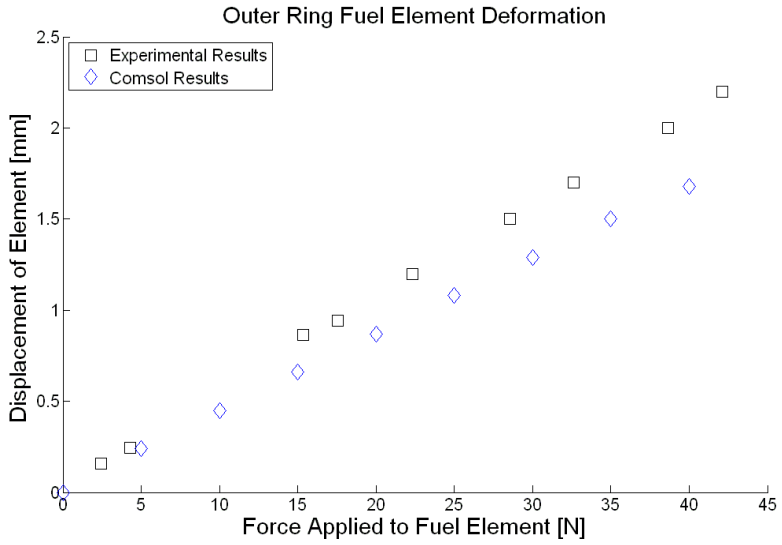

Figure 6 Experimental results of an out of reactor bundle deformation experiment to the results of a simulation of the experiment using the model implemented in Comsol.

The bundle deformation model is therefore demonstrated to be in reasonable agreement with the BOW code and experimental data.

3.3 Preliminary pellet deformation predictions

Preliminary results from the pellet deformation model show that the model is able to predict pellet hour-glassing; however, the magnitude of the calculated deformation has yet to be verified. The calculated displacement in the radial direction throughout the whole model is shown as a surface plot in Figure 7 (a) for a 40 kW m^{-1} case at 200 MWh kgU^{-1}. Figure 7 (b) shows the radial displacement of the sheath surface for five burnups with a linear power of 40 kW m^{-1}. The deformation is initially dominated by densification effects at low burnup; however, at higher burnup fission product swelling begins to dominate.

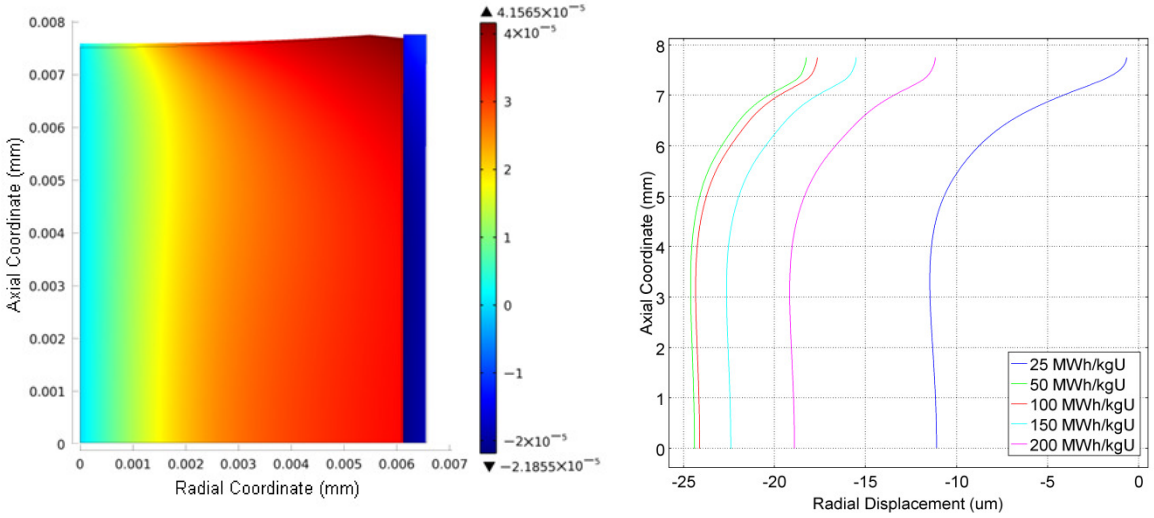

(a) (b)

Figure 7: (a) Surface plot of the radial displacement throughout the pellet and the sheath indicated by the colour scale. (40 kW m^{-1}, 200 MWh kgU^{-1}) and (b) radial displacement of the sheath surface at 5 different burnups (40 kW m^{-1}).

Current work aims to validate this model against other models and available post-irradiation examination (PIE) data.

4. Summary and Conclusions

Three codes/models have been developed to account for intact and defective fuel element performance, bundle deformation, and pellet deformation. The FORCE code displays reasonable agreement with the results of the pre-existing codes ELESTRES and ELESIM, in terms of temperature, gas pressure, and structural deformation. In addition, the FORCE code demonstrates reasonable agreement with previous models and experimental data for fuel oxidation and fission gas release. The fuel element bowing model demonstrates reasonable agreement with the BOW code and experimental measurements for bundle deformation. The pellet deformation demonstrates the ability to account for circumferential ridging of individual pellets, presenting more detailed results for axial variations in fuel and sheath deformation. As the three codes/models are developed using the COMSOL Multiphysics commercial software package, it is possible to link these models to one another as well as other separate effects models developed using the same software.

Acknowledgements

The authors would like to thank J. Higgs, A. El-Jaby, and D. Morgan for their pioneering work on modelling fuel oxidation, fission gas release, and intact fuel element performance at the Royal Military College of Canada. The authors also thank Chalk River Laboratories for providing access to the ELESTRES and ELESIM codes.

References

[1] M. Tayal, AECL Report AECL-9331, 1987.
[2] M.J.F. Notley, *Nucl. Technol.* 44 (1979) p445.
[3] S.D. Yu, M. Tayal, P.N. Singh, Presented at the 4th International Conference on CANDU Fuel, Pembroke, Canada, Oct. 1-4, 1995. pp4B.52-4B.69.
[4] M. Tayal, Nuclear Engineering and Design, 116 (1989) 149.
[5] J. Veeder, M.H. Schankula, *Nuclear Engineering and Design* 29, pp. 167-179, 1974.
[6] B.J. Lewis, F.C. Iglesias, D.S. Cox, E. Gheorghiu, *Nuclear Technology* 92 (1990), 353.
[7] D.R. Olander, *Nuclear Technology*, 74 (1986) 215.
[8] COMSOL Multiphysics Version 3.5a finite element modeling and simulation commercial software, www.comsol.com.
[9] D.R. Olander, *Fundamental Aspects of Nuclear Reactor Fuel Elements*, TID-26711-p1,US. Department of Energy, 1976.
[10] A. El-Jaby, PhD thesis, Royal Military College of Canada, 2009.
[11] G.V. Kidson, *J. Nucl. Mater.* 88 (1980) 299.
[12] S.D. Beck, Battelle Memorial Institute, Report No. BMI-1433, 1960.
[13] O.V. Khoruzhii, S.Yu. Kourtchatov, V.V. Likhanskii, *J. Nucl. Mater.* 265 (1999), 112.
[14] R.J. White and M.O. Tucker, *J. Nucl. Mater.* 118 (1983) 1.
[15] D.G. Martin, *J. Nucl. Mater.* 152 (1988), 94-101.
[16] I.J. Hastings, L.E. Evans, *Journal of the American Ceramics Society* 62 (1979), 217-218.
[17] D.T. Hagerman, NUREG/CR-6150 Vol. 4. (1997).
[18] D. Morgan, MASc thesis, Royal Military College of Canada, 2007.
[19] R.C. Hibbeler, *Mechanics of Materials*, Prentice Hall, Upper Saddle River, New Jersey, 2000.
[20] M.F. Ashby, *Acta Metallurgica* 887 (1972), 20.
[21] H.E. Sills, R.A. Holt, Zirconium in the Nuclear Industry (Fourth Conference), ASTM STP 681, American Society for Testing and Materials, 1979, 325-341.
[22] J.D. Higgs, B.J. Lewis, W.T. Thompson and Z. He, *J. Nucl. Mater.* 366 (2007) 99.
[23] K. Shaheen, and B.J. Lewis, Proceedings of the 2009 Topfuel Conference, Paris, France, 2009.
[24] K. Shaheen, PhD thesis, Royal Military College of Canada, 2011 (in press).
[25] A. El-Jaby, B.J. Lewis, W.T. Thompson, F. Iglesias, and M. Ip, *J. Nucl. Mater.* 399 (2010) 87.
[26] K. Shaheen, A.D. Quastel, J.S. Bell, B.J. Lewis, W.T. Thompson, and E.C. Corcoran, Proceedings of the 11th CNS International Conference on CANDU Fuel, Niagara Falls Ontario, Canada, October 17-20, 2010.
[27] J. Veeder, M.H. Schankula, *Nuclear Engineering and Design*, 29, pp. 167-179, 1974.
[28] "COMSOL Multiphysics Structural Mechanics Module User's Guide, Version 3.5", COMSOL AB, 2008.
[29] B.J. Lewis, W.T. Thompson, M.R. Kleczek, K. Shaheen, M. Juhas, and F.C. Iglesias, *J. Nucl. Mater.* 408 (2011) p209.
[30] R.A. Verrall, Z. He and J. Mouris, *J. Nucl. Mater.* 344 (2005) 240-245.
[31] R.L. da Silva and N. Macici, AECL Report CRNL-2674, 1985.